GFZ
Helmholtz-Zentrum
POTSDAM

Originally published as:

Lesur, V., Wardinski, I., Rother, M., Mandea, M. (2008): GRIMM: the GFZ Reference Internal Magnetic Model based on vector satellite and observatory data. - Geophysical Journal International, 173, 2, pp. 382—394.

DOI: http://doi.org/10.1111/j.1365-246X.2008.03724.x

Geophys. J. Int. (2008) **173,** 382–394 doi: 10.1111/j.1365-246X.2008.03724.x

GRIMM: the GFZ Reference Internal Magnetic Model based on vector satellite and observatory data

Vincent Lesur, Ingo Wardinski, Martin Rother and Mioara Mandea

GeoForschungsZentrum, Potsdam, Germany. E-mail: lesur@gfz-potsdam.de

Accepted 2008 January 3. Received 2007 November 15; in original form 2007 July 11

SUMMARY

In this paper the new GFZ Reference Internal Magnetic Model (GRIMM) is presented. The model has been derived from nearly 6 yr of CHAMP satellite data and 5 yr of observatory hourly means. At high latitudes, full vector satellite data are used at all local times which allows a separation between, on one hand, the fields generated by ionosphere and field aligned currents, and, on the other hand, the fields generated in the Earth's core and lithosphere. This selection technique leads to a data set without gaps during the polar summers resulting in a core field model that has an unprecedented time resolution. The modelled static core field, secular variation and lithospheric field are all in good agreement with previously published magnetic field models. Order five B-splines are used to model the variation in time of the core field. The energy in the secular acceleration has, therefore, a smooth behaviour in time and increases continuously from 2003.5. Mapping the field acceleration from 2001.5 to 2005.5 reveals its rapid and complex evolution over this time period at the Earth's surface. Due to the applied regularization technique, the acceleration energy in spherical harmonics 6–11 is significantly larger than for other models and we show that such a spectrum is acceptable.

Key words: Satellite magnetics.

1 INTRODUCTION

The successive launch of the Ørsted, Champ and SAC-C magnetic survey satellites in the recent years has resulted in a significant improvement in the quality of Earth's magnetic field models. The recently published satellite-based models are POMME-3 (Maus *et al.* 2006), CHAOS (Olsen *et al.* 2006) and its recent extension xCHAOS (Olsen & Mandea 2007b), and BGS/G/L/0706 (Thomson & Lesur 2007). They usually describe the core field and its secular variation, the field generated in the lithosphere and the large-scale external fields assumed to be generated in the magnetosphere. The level of noise in most of these models slowly increases with the spherical harmonic (*SH*) degrees to reach unacceptable values around degree 50 for the lithosphere, around degree 12 for the core field secular variation (*SV*) and at degree 4 or 5 for the core field secular acceleration (SA). The altitude of the CHAMP satellite is low enough and the data dense enough to build higher resolution models and, if we are unable to do so, it is because of the level of noise in the data. This noise is generally attributed to a poor representation of fields varying rapidly in time as are the fields generated in the magnetosphere, in the ionosphere and by field aligned currents (FAC).

With the exception of the BGS model, all the above models use exclusively total intensity (*F*) data over the polar regions. This approach limits in the data set the signal associated with FAC that is mainly in the direction perpendicular to the main magnetic field. The BGS model uses the data component along the direction of a pre-defined field model with the same expected effect. However, as indicated by Le Mouël *et al.* (2003), the signal associated with FAC may not be fully removed by this process. For the ionosphere, the generated magnetic field has a significant component along the main field direction and, therefore, can be clearly seen in *F* data. To limit the ionospheric contributions in these data, the usual approach consists of selecting high latitude *F* data only during the polar winters. This approach has been used successfully to build models from Ørsted, CHAMP and SAC-C data, but it clearly limits their resolution in time at high latitudes as there is no night time data over the polar regions for a large part of the year. It is unlikely that the forthcoming Swarm constellation will help to solve these difficulties, so we therefore, need to use high latitude data at all local times, even during summers when the polar areas are sunlit. Under such conditions vector data are required in order to separate the fields generated in the ionosphere and by FAC from the core and lithosphere magnetic fields. Here we introduce the new GFZ Reference Internal Magnetic Model (GRIMM), built exclusively from vector magnetic data, our main goal being to describe with better temporal resolution the core magnetic field behaviour. We also attempt to reduce the level of noise in mid and low magnetic latitude data by selecting data exclusively in directions where the ring current signal is small. To achieve this, the vector magnetic data, originally in the North, East, Center (NEC) coordinate system, have to be rotated into the Solar Magnetic (SM) Cartesian coordinate

© 2008 The Authors
Journal compilation © 2008 RAS

system (i.e. the system of coordinates where the Z-axis is pointing North along the Earth's dipole axis and the Y-axis is perpendicular to the Earth–Sun line towards dusk) and then data in the Z (SM) direction are rejected.

As the main focus of the new GRIMM model is to describe the core field and its variation in time, we have been particularly careful to build a model with an acceptable behaviour at the core–mantle boundary (CMB). We pay special attention to the years 2002–2005 and see how well the *SV* at the Earth's surface (Mandea & Olsen 2006) and the geomagnetic jerks (Olsen & Mandea 2007a,b) are described by the new model. The time span of validity for this new model is roughly the same as CHAOS or POMME-3. As for CHAOS, or its recently updated version xCHAOS (Olsen & Mandea 2007b), we built a model using B-splines to achieve a high resolution in time. In these latter models, the cubic B-spline core field time parametrization leads to a SA that varies like a degree 1 polynomial in time in between nodes. This is clearly not an ideal parametrization as the amplitude of the acceleration tends to reach a maximum at the node points and then becomes unrealistically large. To circumvent this problem order five B-splines are used in GRIMM (order four B-splines are cubic B-splines). In evaluating GRIMM, comparisons with xCHAOS are systematically shown. Although the parametrization of these models is similar in several aspects, the data sources and the way these data are handled are radically different. Differences are to be expected between the models particularly over polar areas where GRIMM should be more robust. We also expect GRIMM to have a smoother and more realistic evolution of the secular acceleration in time.

As the expressions of the magnetic field in geocentric Cartesian coordinate system are not commonly used, these are given in the next section (see also Winch 1968) together with some properties of the field. The third section is dedicated to the data selection and the next one to the model parametrization and estimation. Results are discussed in the section five, and conclusions are made in the last section.

2 THEORY

In the absence of magnetic sources, the geomagnetic field can be presented as the negative gradient of a potential: $\mathbf{B}_p = -\nabla V(\theta, \phi, r, t)$. The source of this poloidal field can be internal or external in origin, and the associated potentials V_i and V_e, are described on a spherical surface by:

$$V_i(\theta, \phi, r, t) = a \sum_{l,m} \left(\frac{a}{r}\right)^{l+1} g_l^m(t) Y_l^m(\theta, \phi) \tag{1}$$

$$V_e(\theta, \phi, r, t) = a \sum_{l,m} \left(\frac{r}{a}\right)^{l} q_l^m(t) Y_l^m(\theta, \phi), \tag{2}$$

where θ and ϕ are the colatitude and longitude, $a = 6371.2$ km is the reference radius, $Y_l^m(\theta, \phi)$ are the usual Schmidt normalized spherical harmonic (*SH*) functions and $g_l^m(t)$, $q_l^m(t)$ are the Gauss internal and external coefficients. We use here the convention that negative orders ($m < 0$) are associated with $\sin(m\,\phi)$ terms, whereas zero or positive orders ($m \geq 0$) are associated with $\cos(m\,\phi)$.

What follows is divided in three subsections: we justify first different aspects of the data selection technique used at mid and low latitudes, the modelling techniques are then presented for the fields generated by FAC and finally for the fields generated in the high latitude ionosphere.

2.1 Vector component selection at mid and low latitudes

We consider the direction Z of the geocentric Cartesian coordinate system (i.e. $\approx$ the Earth's rotation axis), and assume an optimal distribution of vector data at satellite altitude such that a magnetic field model can be robustly built. Let us consider a data set made of the Z component of the measured magnetic field only. We use here the Z component because the formulae are simpler in that case. As it is explained below, the results obtained are easily derived for any arbitrary directions by rotation. The magnetic field of external origin in this Z direction is given by:

$$\mathbf{B}_{pZ}^e = -\cos\theta\ \partial_r V_e(\theta, \phi, r, t) + \sin\theta\ \frac{1}{r}\partial_\theta V_e(\theta, \phi, r, t) \tag{3}$$

which leads to:

$$\mathbf{B}_{pZ}^e = -\sum_{l=1}^{L}\sum_{m=-l}^{l} \left(\frac{r}{a}\right)^{l-1} q_l^m(t)\sqrt{(l+|m|)(l-|m|)}\ Y_{l-1}^m(\theta, \phi). \tag{4}$$

The external field is generally assumed to be large scale and generated mainly in the magnetosphere which justifies the use of $L = 2$ as the maximum *SH* degree. If we consider only the first degree ($l = 1$), it follows that the normalization factor under the square root vanishes for $m = l$, that only the order $m = 0$ is possible and, therefore, only the *SH* function $Y_0^0(\cos\theta)$ is involved. This function is a constant in space, so as expected, the large scale *SH* degree 1 external field along the Z direction (i.e. associated with q_1^0) is a constant in space. The field of internal origin is given by:

$$\mathbf{B}_{pZ}^i = \sum_{l=1}^{L}\sum_{m=-l}^{l} \left(\frac{a}{r}\right)^{l+2} g_l^m(t)\sqrt{(l+|m|+1)(l-|m|+1)}\ Y_{l+1}^m(\theta, \phi). \tag{5}$$

In this equation for a given degree l the *SH* function is $Y_{l+1}^m(\theta, \phi)$ whereas it was $Y_{l-1}^m(\theta, \phi)$ in the expression (4) of the external field. If the maximum *SH* degree $L = 2$ is an acceptable approximation for the external field, the *SH* function of 'highest' degree in eq. (4) is $Y_1^m(\theta)$,

© 2008 The Authors, *GJI*, **173,** 382–394
Journal compilation © 2008 RAS

whereas in eq. (5) the *SH* function of 'minimum' degree is $Y_2^m(\theta, \phi)$. Therefore, using only the distribution of Z component data described above leads to a separation of the internal and external field contributions to the magnetic field.

It should be noted that the full set of external Gauss coefficients cannot be estimated from Z component data alone: it is clear from eq. (4) that the $q_l^l(t)$ cannot be resolved. However, this same data set gives a unique estimation of the internal Gauss coefficients. This is obvious because the internal Z magnetic field component in eq. (5) is the equation of a band-limited potential on the sphere and the square rooted normalization factor never vanishes for the set range of l and m values. However, having a unique set of internal Gauss coefficients does not mean that all $g_l^m(t)$ are robustly estimated. Following the same approach as in Lowes (1975) and assuming that for all data the errors are uncorrelated and have the same variance, it is easy to estimate the variances $v_z(l, m)$ of the $g_l^m(t)$ computed by least-squares from Z component data:

$$v_z(l, m) \propto \frac{2l + 3}{(l + |m| + 1)(l - |m| + 1)}. \tag{6}$$

The variances of the Gauss coefficients are, therefore, dependent on the *SH* degree and order. The best defined coefficients for a given *SH* degree l are the zonal coefficients (i.e. $m = 0$). They behave asymptotically like $\frac{1}{l}$. On the other hand, variances for sectorial Gauss coefficients (i.e. $m = l$) are asymptotically independent of the degree l. These variances have to be compared with those obtained when the three components of the magnetic data vector are used: $v_{xyz}(l, m) \propto \frac{1}{(l+1)}$ (Lowes 1975). These are independent of the *SH* order m and behave asymptotically like $\frac{1}{l}$. Clearly, the sectorial Gauss coefficients are better resolved at high *SH* degree if the three components of the magnetic vector data are used, compared to the Z component only option.

The above properties are indeed invariant by rotation and there is a similar separation of external and internal contributions if data in the X or Y, or any other constant direction of the Cartesian coordinate system is used. As for the Z component, all the external Gauss coefficients cannot be resolved. For the variances, if one component only is used, some internal Gauss coefficients or combination of Gauss coefficients cannot be robustly estimated. The situation is greatly improved if two of the three components of the vector data are used. We give here the expression for the internal poloidal field in the X and Y directions:

$$\begin{aligned}\mathbf{B}_{pX}^i = &-\frac{1}{2}\sum_{l=1}^{L}\left(\frac{a}{r}\right)^{l+2}\Bigg\{\sqrt{(l+1)(l+2)}g_l^0(t)Y_{l+1}^1(\theta,\phi)\\ &+\sum_{m=1}^{l}\sqrt{(l+m+1)(l+m+2)}\left[g_l^m(t)Y_{l+1}^{m+1}(\theta,\phi)+g_l^{-m}(t)Y_{l+1}^{-m-1}(\theta,\phi)\right]\\ &-\sum_{m=1}^{l}\sqrt{(l-m+1)(l-m+2)}\left[g_l^m(t)Y_{l+1}^{m-1}(\theta,\phi)+g_l^{-m}(t)Y_{l+1}^{-m+1}(\theta,\phi)\right]\Bigg\}\end{aligned} \tag{7}$$

$$\begin{aligned}\mathbf{B}_{pY}^i = &-\frac{1}{2}\sum_{l=1}^{L}\left(\frac{a}{r}\right)^{l+2}\Bigg\{\sqrt{(l+1)(l+2)}g_l^0(t)Y_{l+1}^{-1}(\theta,\phi)\\ &+\sum_{m=1}^{l}\sqrt{(l+m+1)(l+m+2)}\left[g_l^m(t)Y_{l+1}^{-m-1}(\theta,\phi)+g_l^{-m}(t)Y_{l+1}^{m+1}(\theta,\phi)\right]\\ &+\sum_{m=1}^{l}\sqrt{(l-m+1)(l-m+2)}\left[g_l^m(t)Y_{l+1}^{-m+1}(\theta,\phi)-g_l^{-m}(t)Y_{l+1}^{m-1}(\theta,\phi)\right]\Bigg\}.\end{aligned} \tag{8}$$

As before the internal Gauss coefficient variances can be estimated and it is obtained:

$$v_{xy}(l, m) \propto \frac{2(2l + 3)}{(l + |m| + 1)(l + |m| + 2) + (l - |m| + 1)(l - |m| + 2)}. \tag{9}$$

The best defined Gauss coefficients are now the sectorial ($m = l$) and the worst defined are the zonal ($m = 0$), but in both cases their variances behave asymptotically like $\frac{1}{l}$. For all these variance estimates, it is assumed that the noise in the data set is uncorrelated and independent of the direction. This is not the case for real data, and therefore, there are no major disadvantages in using only two components of the vector magnetic data compared with the three-component option. In the data selection process (described below) the component along the internal dipole axis is rejected at mid and low latitudes as it has the largest level of noise due to the usually poorly modelled ring current magnetic field. We use the X and Y (SM) components only which, as shown above, leads to a separation of external and internal large scale magnetic fields and also leads to a robust estimation of the internal Gauss coefficients at all *SH* degrees.

2.2 Modelling toroidal magnetic fields

Over the polar areas it is not possible to use only two vector data components because they are strongly contaminated by the field generated by FAC. At satellite altitude r_s part of this field is toroidal and is given by: $\mathbf{B}_t = -\hat{\mathbf{r}} \times \nabla_{\mathbf{s}}\Psi(\theta, \phi, t)$, where $\hat{\mathbf{r}}$ is the unit vector in the radial direction and $\Psi\ (\theta, \phi, t)$ is given by:

$$\Psi(\theta, \phi, t) = r_s \sum_{l,m}^{L} \alpha_l^m(t) Y_l^m(\theta, \phi). \tag{10}$$

These equations, associated with a radial system of current, lead to a purely tangential field that contains all *SH* degrees up to *L* and, therefore, it cannot be separated easily from the internal field, unless the three components of the vector data are used. The *SH* in eq. (10) can be replaced by a series of localized functions $\mathcal{F}_i(\theta, \phi)$ (see for example, Lesur 2006) defined by:

$$\mathcal{F}_i(\theta, \phi) = \sum_{l,m}^{L} f_l \; Y_l^m(\theta_i, \phi_i) Y_l^m(\theta, \phi), \tag{11}$$

where the f_l are chosen such that the gradients of the function $\mathcal{F}_i(\theta, \phi)$ vanish rapidly away from its centre (θ_i, ϕ_i). If $f_l \neq 0$ for all l and if there is enough of these functions, the expression (10) is equivalent to (see Lesur 2006, for 'exact equivalence' rules):

$$\Psi(\theta, \phi, t) = r_s \sum_i \alpha_i(t) \mathcal{F}_i(\theta, \phi), \tag{12}$$

where the $\alpha_i(t)$ are the coefficients corresponding to the $\alpha_l^m(t)$ in eq. (10). In GRIMM their time dependence that includes a constant term and an annual variation, is defined as:

$$\alpha_i(t) = \alpha_i^0 + \alpha_i^c \frac{1 + \cos(2\pi\, t)}{2} + \alpha_i^s \frac{1 + \sin(2\pi\, t)}{2}, \tag{13}$$

where t is the time in decimal year.

2.3 Modelling the ionospheric fields

Over the polar regions a model of the field generated in the ionosphere is also needed, and assuming the ionospheric currents are all flowing on a thin shell of radius r_{io}, they are defined by: $\mathbf{J}_{io} = -\hat{\mathbf{r}} \times \nabla_s \Phi(\theta, \phi, t)$ where the current function $\Phi\ (\theta, \phi, t)$ is given by:

$$\Phi(\theta, \phi, t) = r_{io} \sum_{l,m}^{L} \beta_l^m(t) Y_l^m(\theta, \phi). \tag{14}$$

These currents generate a poloidal magnetic field that is, therefore, the negative gradient of a potential $V_{io}(\theta, \phi, r)$. It is easy to establish (see for example, Parkinson 1983) that this potential is related to the current function coefficients via:

$$V_{io}(\theta, \phi, r, t) = \begin{cases} \mu_0 r_{io} \sum_{l,m} \frac{l}{2l+1} \left(\frac{r_{io}}{r}\right)^{l+1} \beta_l^m(t) Y_l^m(\theta, \phi) & \text{for } r \geq r_{io} \\ -\mu_0 r_{io} \sum_{l,m} \frac{l+1}{2l+1} \left(\frac{r}{r_{io}}\right)^{l} \beta_l^m(t) Y_l^m(\theta, \phi) & \text{for } r \leq r_{io}, \end{cases} \tag{15}$$

where $\mu_0 = 4\,\pi\ 10^{-7}$ Hm^{-1} is the vacuum permeability. As above, this potential can be written in terms of localized functions:

$$\tilde{\mathcal{F}}_i(\theta, \phi, r) = \begin{cases} r_{io} \sum_{l,m} \frac{l}{2l+1} \left(\frac{r_{io}}{r}\right)^{l+1} f_l \; Y_l^m(\theta_i, \phi_i) Y_l^m(\theta, \phi) & \text{for } r \geq r_{io} \\ -r_{io} \sum_{l,m} \frac{l+1}{2l+1} \left(\frac{r}{r_{io}}\right)^{l} f_l \; Y_l^m(\theta_i, \phi_i) Y_l^m(\theta, \phi) & \text{for } r \leq r_{io} \end{cases} \tag{16}$$

and therefore:

$$V_{io}(\theta, \phi, r, t) = \mu_0 \sum_i \beta_i(t) \tilde{\mathcal{F}}_i(\theta, \phi, r). \tag{17}$$

The time dependence of the coefficients $\beta_i(t)$ is here:

$$\beta_i(t) = \beta_i^0 + \beta_i^c \frac{1 + \cos(2\pi\, t)}{2} + \beta_i^s \frac{1 + \sin(2\pi\, t)}{2}. \tag{18}$$

Separating the ionosphere contributions from the fields generated by the lithosphere or the core requires the full vector data and also a sampling of the field at all local time.

3 DATA SELECTION

The GRIMM model is built using exclusively vector magnetic data. The main motivation for this choice is that we want to use data during polar summers, and, during these summers, vector data at all local times are necessary to separate fields generated by FAC and in the ionosphere from the core and lithospheric fields.

From 2001.0 to 2006.0, CHAMP vector data corrected from orientation errors (i.e. data set version 50 as available from the CHAMP data centre) with acceptable quality flag values are selected between $\pm 55^\circ$ magnetic latitudes such that Interplanetary Magnetic Field (*IMF*) z component B_z has positive values, 20 s minimum separate two data points, the local time (LT) is between 23:00 and 05:00 and the sun is below the horizon up to 100 km above the Earth's reference radius. The Vector Magnetic Disturbance time-series (VMD), an estimate of the disturbances due to the large scale external field (Thomson & Lesur 2007), is also used and data are selected if the VMD norm is no larger than 20nT and the norm of its derivative less than 100 nT d^{-1}. Only the X and Y components in SM coordinate system are used. It was shown in the previous section that using two components only leads to robust estimates of the internal Gauss coefficients and it has the further advantage that there is no need to model the field generated by the symmetric ring current.

At high latitudes only (i.e. magnetic latitudes outside the $\pm 55^\circ$ interval) the three components of the magnetic data vector are used. There is no point using data in SM coordinate system at these latitudes as the ring current is not the main source of noise in the data over polar areas, therefore, the data are used in the usual NEC coordinate system. CHAMP data corrected for orientation errors with acceptable quality flag

© 2008 The Authors, *GJI*, **173,** 382–394
Journal compilation © 2008 RAS

Table 1. Results of the data selection process. The obtained mean residual and rms values are also given.

Data	Mag. Lat. range	Component	N	Mean res. <2006.0	rms <2006.0	Mean res. >2006.0	rms >2006.0
Sat.	$\mid$ mlat $\mid < 55^\circ$	X (SM)	264219	−0.40 nT	3.49 nT	−0.05 nT	4.11 nT
		Y (SM)	264219	−0.63 nT	4.04 nT	−0.44 nT	5.63 nT
	$\mid$ mlat $\mid > 55^\circ$	North	603945	0.27 nT	51.84 nT	−1.95 nT	56.56 nT
		East	603945	0.98 nT	58.36 nT	1.53 nT	61.57 nT
		Centre	603945	−0.77 nT	21.30 nT	−1.81 nT	24.55 nT
Obs.	$\mid$ mlat $\mid < 55^\circ$	X (SM)	196468	0.05 nT	3.28 nT		
		Y (SM)	196468	0.06 nT	3.57 nT		
	$\mid$ mlat $\mid > 55^\circ$	North	64354	−2.03 nT	22.35 nT		
		East	64354	0.08 nT	13.27 nT		
		Centre	64354	0.61 nT	18.71 nT		

values are selected for positive *IMF* B_z values, with 20 s minimum between two data points, a VMD norm no larger than 20 nT and the norm of its derivative less than 100 nT d^{-1}. No selection is applied on LT or Sun position. The use of the full magnetic vector at all local times is necessary for separating the field generated by FAC or in the ionosphere from the fields of internal origin. Using the full vector data at high latitude also improves the robustness of the low order internal Gauss coefficients, in the same way that vector data are used at mid-latitudes to avoid the Backus effect in models built mainly from scalar magnetic data (Backus 1970).

At all latitudes, observatory hourly mean values are selected following the same criteria as satellite data for low and midlatitudes. Three component vector data in the NEC are used at high latitudes while, between $\pm 55^\circ$ magnetic latitudes only X and Y (SM) data are used.

At the time of this study, for year 2006, no observatory hourly mean values were available and the *IMF* strength and direction information were rarely available after July. The VMD was not computed yet, and the Dst index was available only as provisional values. The satellite data for year 2006 were, therefore, selected between $\pm 55^\circ$ magnetic latitudes with 20 s minimum between two data points, for LT between 23:00 and 05:00 and for the sun below the horizon up to 100 km above the Earth's reference radius. The data were also selected for provisional Dst values in the range ± 20 nT and their derivatives in time between ± 10 nT hr^{-1} until modified Julian day 2420.0 (i.e. 2006 August 16) and then, as the provisional Dst drifts towards negative values, the bounds on Dst values were set to $[0: -40]$ nT. Only the X and Y components in *SM* coordinate system were used. At high latitudes the full magnetic vector data were used in the NEC coordinate system and the selection criteria were the same as above, but without selection applied on local time or Sun position. We comment that for year 2006 the selection process is not satisfactory and the level of noise in these data is necessarily larger than for the previous years.

The number and type of data values used are given in Table 1.

4 MODEL PARAMETRIZATION AND ESTIMATION

The data selection process described in the previous section does not allow a robust modelling of the large scale external field. We describe this field as the gradient of a scalar potential (eq. 2). The maximum *SH* degree used is $L = 1$ (although $L = 2$ would have been possible) and the time dependence of each Gauss coefficient is a piecewise continuous linear polynomial with a node every 3 months. For mid and low latitude data only, a dependence on the VMD index is introduced via a scaling factor. Independent scaling factors are used for satellite and observatory data. Even if, in principal, only one scaling factor is needed here, two were used in order to minimize the noise level in satellite data. The fit to satellite data improves with two scaling factors which ultimately is beneficial for the resolution in space of the core and lithospheric field models. Scaling factors are introduced also for the internal part of the VMD describing the field induced in the Earth by the large scale external field. Altough the VMD is based only on a 1-D Earth conductivity model, we would not expect improvements to the results by using a 3-D conductivity model instead. We did not use a VMD dependence for polar data as their very high level of noise precludes a realistic estimate of the large scale external field there. A poor estimate of these fields results in an increase in satellite data noise level at mid and low latitudes. As above, this increase has a detrimental effect on the core and lithosphere model resolution. No VMD dependence is applied for year 2006 as the VMD index is not available for that year.

The data selection criteria at high latitude leads to a very good separation of the fields generated by FAC from the fields generated in the Earth's core and lithosphere. The FAC generate toroidal fields, and there are no difficulties in separating them from poloidal fields. These toroidal fields are modelled using a scalar potential (eq. 12) where the function centres are defined in SM coordinate system and the time dependence, given in eq. (13), includes a constant term and an annual periodicity.

As for toroidal fields, the fields generated in the ionosphere apparently separate well from the fields due to internal sources. This happens because the average field generated in the ionosphere has a geometry varying slowly in a coordinate system linked to the sun and, therefore, average out in a coordinate system rotating with the Earth. The model for these fields is using a current function leading to a scalar potential as in eqs (16) and (17) with a reference radius of 6481.2 km (i.e. 110 km above the Earth's reference radius). As above the function centres are defined in SM coordinate system and the time dependence is defined in eq. (18).

The localized functions used for these two fields (eqs 11 and 16) have a maximum *SH* degree $L = 40$ and their centres are nearly equidistant on the sphere (Chambodut *et al.* 2005). Only the 920 functions that are centred on magnetic latitudes outside the interval $\pm 55^\circ$

Table 2. B-spline node positions.

Node number	Date
1-5	2001.0
6	2001.614
7	2002.710
8	2003.778
9	2004.872
10	2005.940
11–15	2006.726

are used. The above parametrization leads to models with limited time resolution, however, we will see as we proceed that models of fields generated in the ionosphere and by FAC are not required in order to build accurate and robust models of the core and lithospheric fields.

As described in Section 2 the core and lithospheric fields are gradients of scalar potentials. The general form of the potential is given in eq. (1). For a given set of Gauss coefficients, the vector magnetic field can be computed and then rotated to the direction corresponding to a given data value. From degree 1 to 14, the time dependence is defined by order 5 B-splines and the node positions given in Table 2 are roughly 400 days apart. The positions of these nodes correspond to time periods where CHAMP data, selected following the criteria given in Section 3, are available at all latitudes. The effect of this choice is seen in more robust estimates of the SA. Above *SH* degree 14 and up to the maximum degree $L = 60$, the Gauss coefficients are assumed to be time independent.

The observatory data are modelled in the same way as satellite data altough observatory crustal biases are introduced to account for the lithospheric field in each observatory components, and moreover the contributions from FAC or the ionosphere are neglected.

The second time derivatives of the Gauss coefficients are not robustly estimated for the highest degree of the core magnetic field model. Therefore, we constrain the solution to minimize the integral over the sphere and time of the squared second time derivative of the radial magnetic field component at the CMB:

$$I = \int_{t_1}^{t_2} \int_{S(c)} \left| \frac{\partial^2 \mathbf{B}_r^i}{\partial t^2} \right|^2 \mathrm{d}s \; \mathrm{d}t, \tag{19}$$

where $S(c)$ is a spherical surface of radius $c = 3485$ km, the estimated radius of the core, and t_1, t_2 are the limits of the model time span. As the core magnetic field is described by order 5 B-splines, between two spline nodes the second time derivative of the field is a quadratic polynomial and the time integral is calculated exactly using a three points Gaussian rule. The *SH* degrees and orders are separated by the surface integral and, therefore, eq. (19) leads to a block diagonal damping matrix. The balance between fit to the data and smoothness of the solution in time is controlled via a damping parameter that is here set to 1.10^{-3}. We comment that this is a relatively weak smoothing and the damping mainly affects the high *SH* core field Gauss coefficients. In particular this regularization does not significantly affect the first 5 *SH* degree Gauss coefficients. This is different from the regularization introduced for CHAOS (Olsen *et al.* 2006), where the same norm is minimized but at the Earth's reference radius.

The constraint introduced above controls the SA well when cubic B-splines are used, but, using order 5 B-splines introduces further degrees of freedom in the model. This affects all the first 14 *SH* degrees, but is mainly visible in the low degrees where the regularization introduced by minimizing eq. (19) has no effect. To circumvent this problem we also minimize the norm of the third time derivative of the radial component of the field over a sphere at the Earth's reference radius ($a = 6371.2$ km):

$$J = \int_{t_1}^{t_2} \int_{S(a)} \left| \frac{\partial^3 \mathbf{B}_r^i}{\partial t^3} \right|^2 \mathrm{d}s \; \mathrm{d}t. \tag{20}$$

The damping parameter is set to $5 \times 10^{+2}$ and mainly the low *SH* degrees are affected. We tested other regularization schemes like imposing a zero SA at the model end points in time, but the results are essentially the same as those presented in the next section. We also tried to introduced, at known jerk epochs, discontinuities in the second derivative in time of the magnetic field. This idea was abandoned as it led to a degradation of the *SV* time behaviour.

Fitting the data by adjusting the Gauss coefficients is a linear inverse problem. The Gauss coefficients are estimated by an iterative reweighted least squares procedure using an $\mathcal{L}_1$ norm (Farquharson & Oldenburgh 1998). The weights associated with data points are the inverse of the data density in areas defined by nearly regular triangles. These weights are also divided by the data variances, but we note that these have little effect on the solution obtained through the iterative reweighted least squares process. These data variances are estimated by several test-runs prior to the final modelling effort.

The final model is obtained by first fitting the core, lithosphere, large scale external and associated induced field models to the data. In a second step the residuals are used to build the ionosphere and toroidal models. Although there is no apparent leakage of the ionospheric fields inside the core field model, the model used for the former fields has too much freedom and cannot be well separated from the core and lithospheric field models. Co-estimation of the ionospheric model together with other internal field models is not possible unless progresses are made in the parametrization of the ionosphere current system. Table 1 also gives the residual rms and mean values for the different data types. Values for year 2006 are given independently as they are significantly larger than for the previous years. We observe that at mid and low latitudes the rms values and the mean values of the residuals are small. For satellite data, the offset absolute values are less than 0.7 nT

© 2008 The Authors, *GJI*, **173,** 382–394
Journal compilation © 2008 RAS

for both X and Y components in SM coordinate system. Such an offsets are associated to a 24-hr periodicity in a coordinate system rotating with the Earth and are, therefore, likely to be linked to a large scale external field. However we have not been able to build an acceptable *SH* degree 1 model that fits these signals well. At high latitudes the noise level is very high, particularly in satellite data. The above mentioned modelling of the field generated in the ionosphere or by FAC does not lead to a significant reduction of these rms values. When a $\mathcal{L}_2$ norm is used during the least squares process, the mean residual values of observatory data are null because the crustal biases absorb any unmodelled contributions. Therefore, as a $\mathcal{L}_1$ norm is used here, the large mean residual values obtained mainly show that the residual distribution is not Gaussian.

5 RESULTS AND DISCUSSION

Fig. 1 presents the field generated by the ionosphere at 400 km altitude as modelled with our parametrization. Fig. 2 shows the toroidal field generated at satellite altitude by FAC. Not many details can be seen and a better time resolution is required in order to build useful models. We note however that the northern cap model seems to present more robust features.

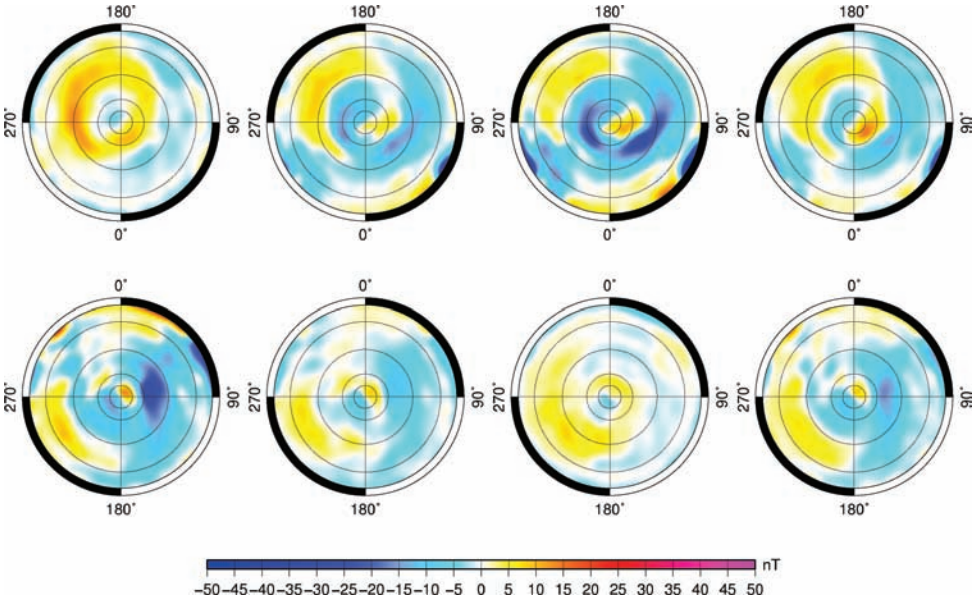

Figure 1. North component of the average ionospheric field estimated for 2003.0, 2003.25, 2003.5 and 2003.75 (from left to right) at the satellite altitude. Top row: Northern polar cap (in SM), bottom row: Southern polar cap (in SM). The X (SM) axis is in the Sun direction at 0°, 90° is dusk.

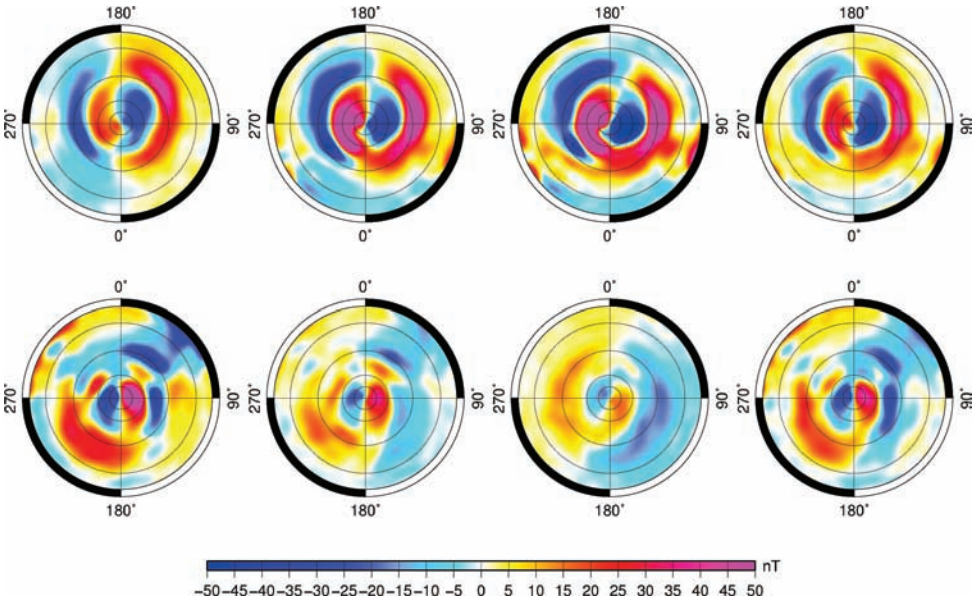

Figure 2. East component of the average toroidal field estimated for 2003.0, 2003.25, 2003.5 and 2003.75 (from left- to right-hand side) at satellite altitude. Top row: Northern polar cap (in SM), bottom row: Southern polar cap (in SM). The X (SM) axis is in the Sun direction at 0°, 90° is dusk.

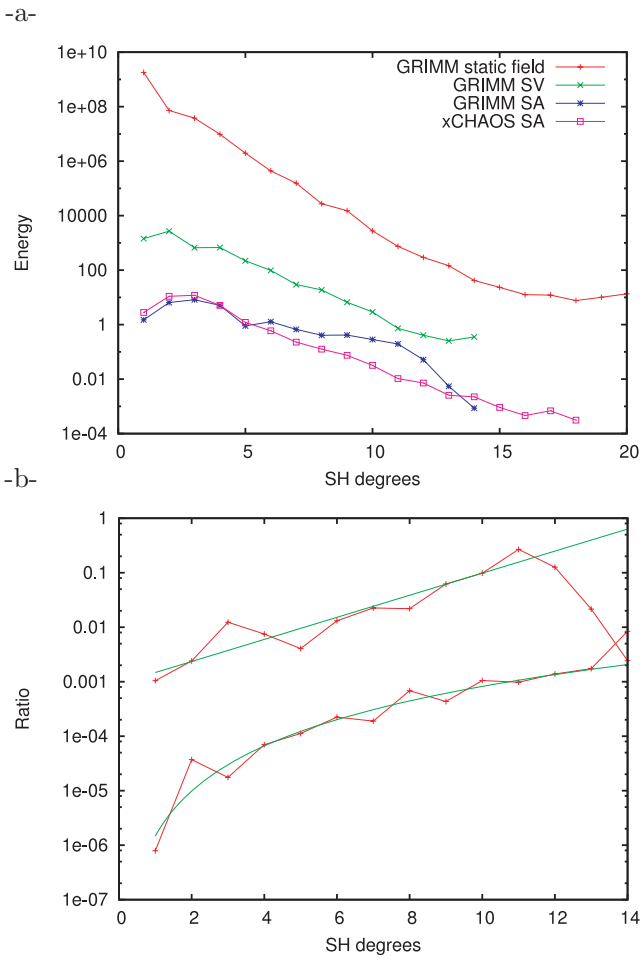

Figure 3. (a) Power spectra of the core field, its secular variation and secular acceleration for year 2003.25 at Earth's reference radius. The acceleration power spectrum is compared with xCHAOS secular acceleration spectrum for the same date. (b) Degree by degree ratio of the power in secular variation to the power in core field (bottom curve) and to the power in secular acceleration to that in secular variation (top curve). Also shown are power law and exponential law fits.

Fig. 3(a) presents the power spectra at the Earth's reference radius ($a = 6371.2$ km) of the derived internal field up to *SH* degree 20, of the core field *SV* and of the SA for year 2003.25. The values associated with the constant part of the field are not different from those obtained for recent geomagnetic models, reaching a minimum at *SH* degree 18. The *SV* behaves as expected up to *SH* degree 12 above which the model is likely to be not reliable. Finally, the SA spectrum has values similar to those of xCHAOS for the first few *SH* degrees, presents larger values than usually obtained from *SH* degrees 5–11, and otherwise is controlled by the regularization process above *SH* degree 11.

Technically, the SA power at the intermediate *SH* degrees (i.e. degrees 5–11) is larger than in xCHAOS because only a weak regularization has been applied here. Models built with other temporal basis functions (e.g. Lesur *et al.* 2005; Maus *et al.* 2006) systematically present a very small acceleration amplitude that is likely to be due to a lack of time resolution. The GRIMM SA is well constrained up to *SH* degree 5 or 6 by the combination of observatory and satellite data. For *SH* degrees above that limit, the observatory data have little effect and the acceleration is controlled solely by satellite data. To assess if the obtained values are acceptable we consider the degree by degree ratio of the power in *SV* to that in the main field (Holme & Olsen 2006):

$$R(l) = \frac{\sum_{m=-l}^{l} (\dot{g}_l^m)^2}{\sum_{m=-l}^{l} (g_l^m)^2}, \tag{21}$$

and also the degree by degree ratio of the power in SA to that in the *SV*:

$$S(l) = \frac{\sum_{m=-l}^{l} (\ddot{g}_l^m)^2}{\sum_{m=-l}^{l} (\dot{g}_l^m)^2}. \tag{22}$$

Both $R(l)$ and $S(l)$ are plotted against *SH* degree l in Fig. 3(b). A power law fit to $R(l)$ and an exponential fit to $S(l)$ for *SH* degree $l = 1$ to $l = 11$ are also plotted. The power law fit to $R(l)$ is better than an exponential fit. This is consistent with an hypothesis of a difference of spectral content between *SV* and static core field (Holme & Olsen 2006). It is found $R(l) \approx 1.47\,10^{-6}\,l^{2.75}$ which leads to a correlation time (Hulot & Le Mouël 1994) $\tau\ (l) = 824.8\,l^{-1.375}$. This power law fit is not much different than what was found for CHAOS (Olsen *et al.* 2006) or in (Holme & Olsen 2006). For the SA the exponential fit is better than a power law fit and is found to be $S(l) \approx 9.26\,10^{-4} \exp(0.47l)$. Whereas

© 2008 The Authors, *GJI*, **173,** 382–394
Journal compilation © 2008 RAS

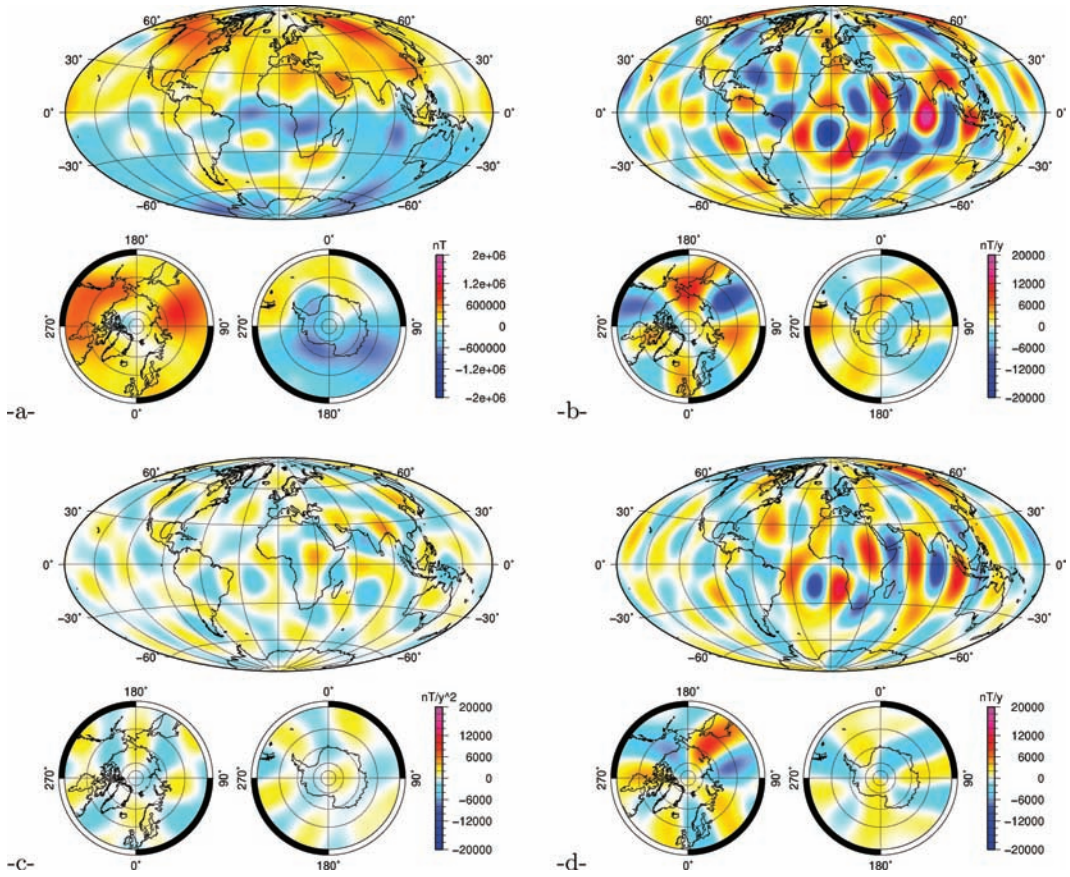

Figure 4. (a) Vertical down component of the modelled core magnetic field at the CMB for 2003.25. (b) Same for the secular variation. (c) Same for the secular acceleration. (d) East component of the modelled core magnetic field secular variation at the CMB for 2003.25.

a lot of theoretical work has been done to estimate what the *SV* spectrum should be (e.g. Voorhies 2004, and references included), nothing has been done for the SA spectrum. This task is far beyond the scope of this paper and we just note that the $S(l)$ exponential behaviour is close to what is observed for $R(l)$ and that may be an indication that the power of acceleration is not overestimated in this model. We also note that extrapolating this exponential behaviour to higher degrees up to a ratio equal to 1, gives an acceleration energy at *SH* degree $l \approx 15$ of roughly the same magnitude as the *SV* energy. Accounting for some possible error in slope, this nicely explains why it is so difficult to estimate reliable *SV* over *SH* degree $l = 12$. At higher *SH* degrees, *SV* models are then necessarily time averages.

In Fig. 4 the vertical down component of the core field and *SV* models, truncated to *SH* degree 12, are plotted for 2003.25 at the CMB. The static core field does not differ significantly from what is given by xCHAOS. The same extrema and reverse flux patches are observed. The *SV* again is very similar to xCHAOS. However, we observe that over the northern polar cap and from 2003.0, GRIMM presents different patterns. These are better seen in the East component plotted in Fig. 4(d). There is a clear set of four minima and maxima just outside the limit of the tangent cylinder ($\sim 28.7^\circ$).

A geomagnetic jerk is seen as a sharp change in *SV* slope in observatory data or, equivalently, is a discontinuity in otherwise nearly constant SA. The SA, as modelled by GRIMM and its evolution in time, is therefore, a useful tool for studying jerks if one occurs during the period covered by the model. The Fig. 4(c) shows the vertical down component of SA at the CMB. An area of strong acceleration sits at the latitudes and longitudes of India, close to the area of the 2003 jerk (Olsen & Mandea 2007a). This strong acceleration pattern drifts south-west between 2002.5 and 2003.5 and vanishes shortly after 2003.5. We interpret this as a tight relation between this acceleration feature and the geomagnetic jerk that occurred around 2003. At the CMB, the SA is, as the *SV*, very weak under the Pacific. The coherency of the modelled SA at the CMB is another indication that the SA power in Fig. 3 is not overestimated. The temporal evolution of the acceleration vertical down component at the Earth's reference radius is plotted in Fig. 5 from 2002.0 to 2005.5, every half year. It shows a positive extremum over India slowly drifting East first, then South to reach western Australia around 2005.0 and then slightly West. This positive anomaly split in two around 2003.5 with a weaker part drifting North-East towards Eastern Siberia and then starts drifting West. An area of negative acceleration appears over South West Africa around 2004.5 and then grow to encompass South Africa in 2005.5. After this date the acceleration pattern may not be as reliable due to the absence of observatory data from 2006.0. The evolution of these patterns is in agreement to the observed jerks around 2003 and 2005.

Fig. 6 shows the changes in acceleration (i.e. the third time derivative of the core field) for 2003.5 and 2004.5. Although the model of the third time derivatives is not very robust, we see in both cases that the maximal changes of acceleration are located at the positions of the jerks

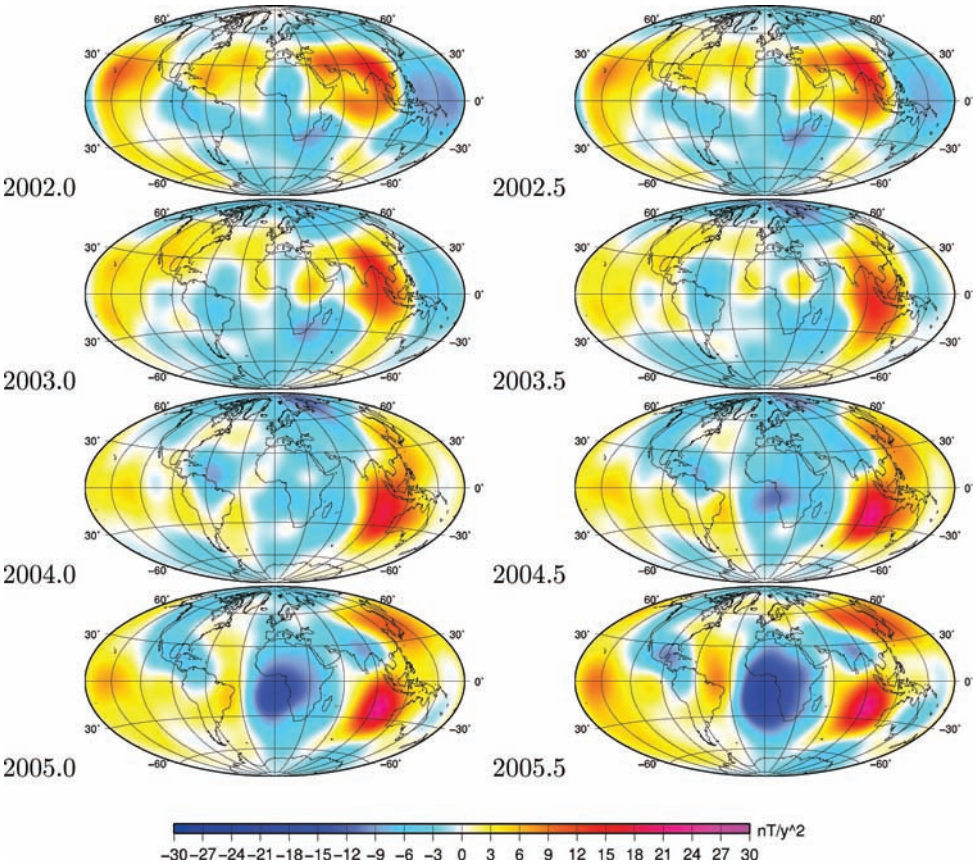

Figure 5. Vertical down component of the modelled secular acceleration at the Earth's reference radius.

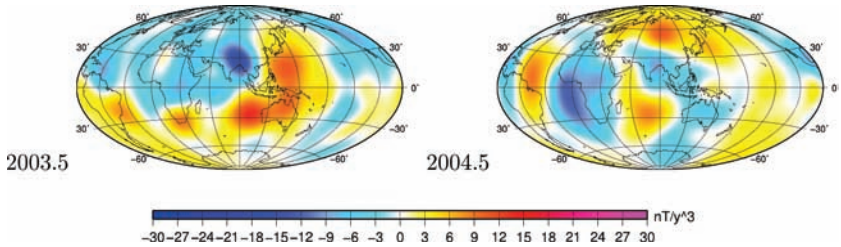

Figure 6. Vertical down component of the third time derivative of the modelled core field at the Earth's reference radius. The central meridian is at 90° degree East.

around 2003 and 2005 (Olsen & Mandea 2007a,b). These two plots are very similar, although with smaller scale features, to the ones given by Olsen & Mandea (2007b). For 2003.5 there is a minimum over India and a maximum over Australia with an extension towards Japan. Also seen are two maxima over South-Africa and Brazil. These two maxima form a single maximum on southern Atlantic in xCHAOS. For 2004.5, as in xCHAOS the large minimum over Southern Atlantic and South Africa is flanked on both sides by maxima. A maximum is also present over Siberia. Whereas in Olsen & Mandea (2007b) the shown plots are differences of acceleration, here are shown third time derivatives of the GRIMM core field model.

It is also interesting to look at the variation in time of the SA energy. This is plotted at the Earth's reference radius for GRIMM and xCHAOS in Fig. 7. The energy for xCHAOS has strong spikes at its B-spline node positions. As described in introduction, cubic B-splines for the core field lead to a linear behaviour of the SA between spline nodes and, therefore, the SA amplitude reaches maxima at these node positions. Little can be done against this and the same difficulty arises for GRIMM in the third time derivative. However, for GRIMM the SA energy varies smoothly and increases after 2003. This increase is robust, but after 2005.5 the time behaviour of GRIMM is questionable as there are no observatory data for year 2006. Overall it seems that there is little agreement between xCHAOS and GRIMM in terms of SA energy. The SA energy at the Earth's surface is mainly controlled by the three first *SH* degrees. The differences between xCHAOS and GRIMM are mainly due to the *SH* first degree, and more specifically the g_1^0 Gauss coefficients that vary more rapidly in xCHAOS. The regularization introduced in GRIMM by minimizing eq. (20) imposes a smooth temporal behaviour for the SA.

© 2008 The Authors, *GJI*, **173,** 382–394
Journal compilation © 2008 RAS

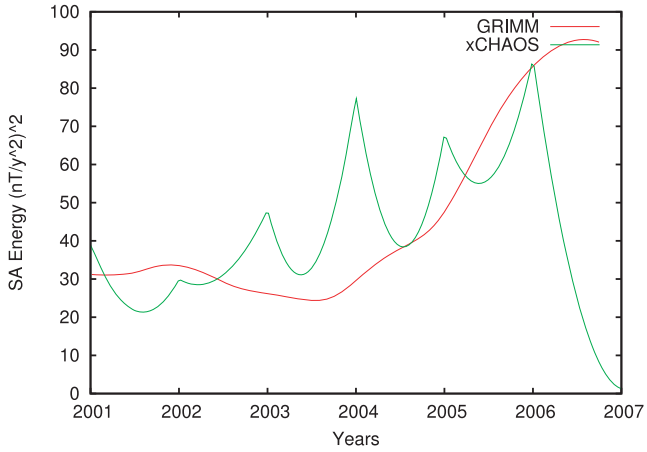

Figure 7. Secular acceleration energy as a function of time at the Earth's reference radius.

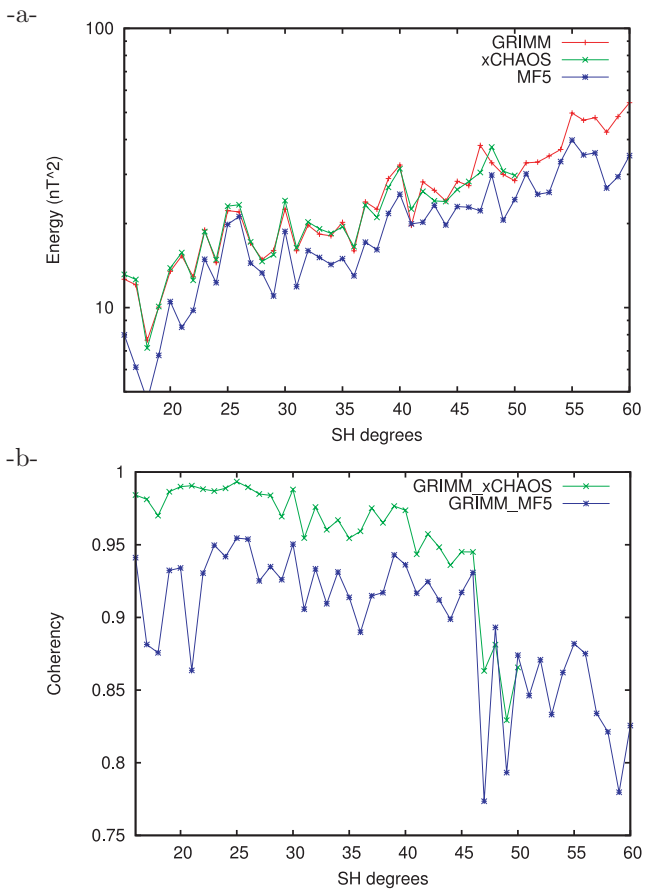

Figure 8. (a) Power spectra of GRIMM, CHAOS and MF5 at the Earth reference radius for *SH* degrees 16–60. (b) Corresponding coherency.

Fig. 8 shows the GRIMM, xCHAOS and MF5 power spectra for *SH* degrees 16 to 60 and their degree correlation. Both GRIMM and xCHAOS models are focused on the core field. We observe nonetheless that they present similar spectra and high correlation up to *SH* degree 45. This is an improvement compared to the correlation between CHAOS and the BGS/G/L/0706 model (Thomson & Lesur 2007). The main differences between GRIMM and xCHAOS lithospheric models are close to the auroral electrojets. The equatorial electrojet has no influence as only night time data are used here. The relatively low coherency between GRIMM and MF5 clearly confirms that not only the MF5 lacks power but also presents spurious features at these low degrees. Fig. 9 present the vertical down component of the GRIMM lithosphere field modelled at the Earth's surface for *SH* degree 16–45 and its differences relative to MF5. The shape of these spurious anomalies are typical of those introduced by along track filtering.

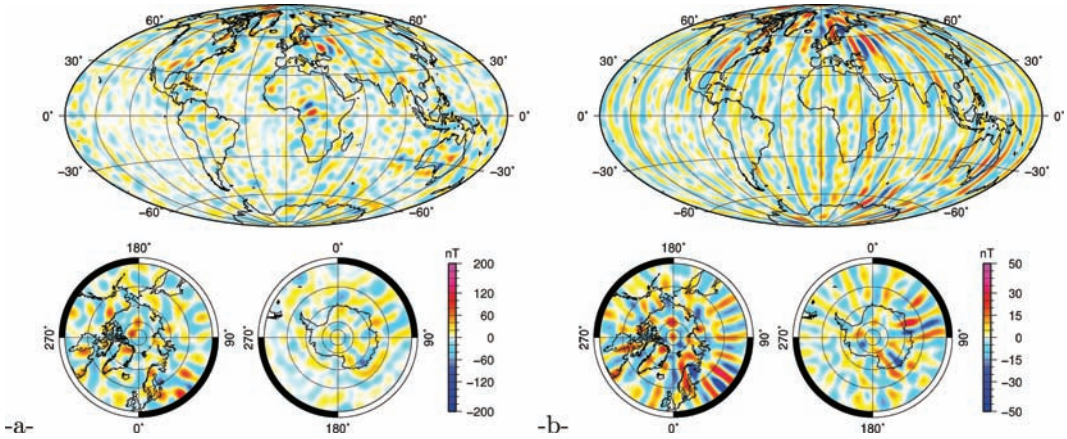

Figure 9. (a) Vertical down component of the GRIMM lithosphere field for *SH* degrees 16–45 at the Earth's reference radius. (b) Vertical down component of the model difference with MF5 for *SH* degrees 16–45 and at Earth's reference radius.

6 CONCLUSION

GRIMM results from the processing of nearly 6 yr of CHAMP satellite data and 5 yr of observatory hourly means. Our data selection approach differs from other models as we are not using night side total intensity data over the polar regions but three-component vector data at all local times. We also used *X* and *Y* SM component vector data at mid and low latitudes, avoiding the need to model the magnetic perturbation generated by the symmetric ring current. The modelling technique is also improved by introducing order 5 B-splines to model the core magnetic field temporal variations while keeping a short time span between B-spline nodes. We also attempted to model the field generated by the field aligned currents and the ionospheric fields, but more work is needed there.

The static core field and secular variation models are in good agreement with other geomagnetic models. Interestingly, the GRIMM secular variation model presents some intriguing features over the northern polar area from 2003.25 which could be linked with core flow dynamics. A major improvement over all previously published models arises from the use of order 5 B-splines in the description of the secular acceleration and its time variation. There are strong indications that the secular acceleration amplitude may have been underestimated in previous models. For the first time we are able to map the temporal evolution of the acceleration patterns at the Earth's surface. They evolve rapidly in a continuous way that is consistent with the observed geomagnetic jerks. The acceleration presents a minimum energy in the year 2003 and rise continuously after that. We hope that a better understanding of geomagnetic jerks will come from the detailed study of the core field acceleration.

ACKNOWLEDGMENTS

We would like to acknowledge the CHAMP data centre and those involved in the CHAMP data processing. We would like also to thank the institutes providing the different indices used in the data selection process as well as the scientists working at magnetic observatories. Many helpful discussions with H. Lühr and N. Olsen are gratefully acknowledged. We thanks also the two reviewers for their helpful comments.

REFERENCES

Backus, G., 1970. Non-uniqueness of the external geomagnetic field determined by surface intensity measurements, *J. geophys. Res.,* **75,** 6339–6341.

Chambodut, A., Panet, I., Mandea, M., Diament, M., Holschneider, M. & Jamet, O., 2005. Wavelet frames: an alternative to spherical harmonic representation of potential fields, *Geophys. J. Int.,* **163,** 875–899, doi:10.1111/j.1365-246X.2005.02754.x.

Farquharson, C. & Oldenburgh, D., 1998. Non-linear inversion using general measures of data misfit and model structure, *Geophys. J. Int.,* **134,** 213–227.

Holme, R. & Olsen, N., 2006. Core surface flow modelling from high-resolution secular variation, *Geophys. J. Int.,* **166**(2), 518–528, doi:10.1111/j.1365-246X.2006.03033.x.

Hulot, G. & Le Mouël, J., 1994. A statistical approach to the Earth's main magnetic field, *Phys. Earth planet. Int.,* **82,** 167–183.

Le Mouël, J., Mayaud, P. & Shebalin, P., 2003. Magnetic activity inside the auroral zones and field-aligned currents, *C.R. Geosci.,* **335,** 935–941, doi:10.1016/j.crte.2003.09.04.

Lesur, V., 2006. Introducing localized constraints in global geomagnetic field modelling, *Earth Planets Space,* **58,** 477–483.

Lesur, V., Macmillan, S. & Thomson, A., 2005. The BGS magnetic field candidate models for the 10th generation IGRF, *Earth Planets Space,* **57,** 1157–1163.

Lowes, F., 1975. Vector errors in spherical harmonic analysis of scalar data, *Geophys. J. R. astr. Soc.,* **42,** 637–651.

Mandea, M. & Olsen, N., 2006. A new approach to directly determine the secular variation from magnetic satellite observations, *Geophys. Res. Lett.,* **33**(L15306), doi:10.1029/2006GL026616.

Maus, S., Rother, M., Stolle, C., Mai, W., Choi, S., Lühr, H., Cooke, D. & Roth, C., 2006. Third generation of the Potsdam Magnetic Model of the Earth (POMME), *Geochem. Geophys. Geosyst.,* **7,** doi:10.1029/2006GC001269.

Olsen, N. & Mandea, M., 2007a. Investigation of a secular variation impulse using satellite data: The 2003 geomagnetic jerk, *EPSL,* **255,** 94–105,

doi:10.1016/j.epsl.2006.12.008.

Olsen, N. & Mandea, M., 2007b. Rapid changing flows in the Earth's core, *Nature Geoscience,* submitted.

Olsen, N., Lühr, H., Sabaka, T., Mandea, M., Rother, M., Tøffner-Clausen, L. & Choi, S., 2006. Chaos–a model of the Earth's magnetic field derived from CHAMP, Ørsted, and SAC-C magnetic satellite data, *Geophys. J. Int.,* **166,** 67–75, doi:10.1111/j.1365-246X.2006.02959.X.

Parkinson, W., 1983. *Introduction to Geomagnetism*, Scottish Academic Press Ltd. Edinburgh, UK.

Thomson, A. & Lesur, V., 2007. An improved geomagnetic data selection algorithm for global geomagnetic field modelling, *Geophys. J. Int.,* **169,** 951–963, doi:10.1111/j.1365-246X.2007.03354.x.

Voorhies, C., 2004. Narrow-scale flow and a weak field by the top of the Earth's core: Evidence from Ørtsed, Magsat, and secular variation, *J. geophys. Res.,* **109,** B03106, doi:10.1029/2003JB002833.

Winch, D., 1968. Analysis of the geomagnetic field by means of cartesian components, *Phys. Earth planet Inter.,* **1,** 347–360.